sustainability

MDPI

Article

Spatial–Temporal Characteristics of Freezing/Thawing Index and Permafrost Distribution in Heilongjiang Province, China

Chengjie Song [1,2,3], Changlei Dai [1,2,3,*], Yaqi Gao [1,2,3], Chuang Wang [1,2,3], Miao Yu [3,4,5], Weiming Tu [1,2,3], Minghui Jia [1,2,3] and Ruotong Li [1,2,3]

1 Institute of Groundwater in Cold Regions, Heilongjiang University, Harbin 150080, China
2 School of Hydraulic and Electric-Power, Heilongjiang University, Harbin 150080, China
3 China and Russian Cold Region Hydrology and Water Conservancy Engineering Joint Laboratory, Heilongjiang University, Harbin 150080, China
4 Faculty of Geology and Survey, North-Eastern Federal University, Yakutsk 677000, Russia
5 Melnikov Permafrost Institute of the Siberian Branch of the Russian Academy of Science, Yakutsk 677000, Russia
* Correspondence: 2006003@hlju.edu.cn

Abstract: Under the trend of climate warming, the high-latitude permafrost in Heilongjiang Province is becoming seriously degraded. The question of how to quantitatively analyze the spatial and temporal trends of multi-year permafrost has become fundamental for current permafrost research. In this study, the temporal and spatial variations of annual mean air temperature (MAAT), annual mean ground temperature (MAGST) and freezing/thawing index based on air and surface temperature data from 34 meteorological stations in Heilongjiang Province from 1971–2019, as well as the variation characteristics of permafrost distribution, were analyzed based on the freezing index model. The results showed that both MAAT and MAGST in Heilongjiang Province tended to decrease with the increase of altitude and latitude. For interannual variation, the MAAT and MAGST warming rates tended to be consistent across Heilongjiang Province, with multi-year variation from −8.64 to 5.60 °C and from −6.52 to 7.58 °C, respectively. From 1971–2019, the mean annual air freezing index (AFI) and ground surface freezing index (GFI) declined at −5.07 °C·d·a^{-1} and −5.04 °C·d·a^{-1}, respectively, whereas the mean annual air thawing index (ATI) and ground surface thawing index (GTI) were elevated at 7.63 °C·d·a^{-1} and 11.89 °C·d·a^{-1}, respectively. The spatial distribution of the multiyear mean AFI, ATI, GFI and GTI exhibited a latitudinal trend, whereas the effect of altitude in the northern mountainous areas was greater than that of latitude. Permafrost was primarily discovered in the Daxing'an and Xiaoxing'an Mountains in the north, and sporadically in the central mountainous regions. The southern boundary of permafrost shifted nearly 2° to the north from 1970 to 2010s, while the southern boundary of permafrost in Heilongjiang Province was stable at nearly 51° N. The total area of permafrost narrowed from 1.11 × 10^5 km^2 in the 1970s to 6.53 × 10^4 km^2 in the 2010s. The results of this study take on a critical significance for the analysis of the trend of perennial permafrost degradation at high latitudes in Heilongjiang Province and the whole northeastern China, as well as for mapping the distribution of large areas of permafrost using the freezing index model. This study provides a reference for natural cold resource development, ecological protection, climate change and engineering construction and maintenance in permafrost areas.

Keywords: Heilongjiang province; freezing/thawing index; permafrost; spatial–temporal distribution; southern boundary of permafrost

check for updates

Citation: Song, C.; Dai, C.; Gao, Y.; Wang, C.; Yu, M.; Tu, W.; Jia, M.; Li, R. Spatial–Temporal Characteristics of Freezing/Thawing Index and Permafrost Distribution in Heilongjiang Province, China. *Sustainability* **2022**, *14*, 16899. https://doi.org/10.3390/su142416899

Academic Editors: Feng Zhang, Rui Zhang, Weiguang Zhang, Ruxin Jing and Chuang Lin

Received: 25 November 2022
Accepted: 13 December 2022
Published: 16 December 2022

Publisher's Note: MDPI stays neutral with regard to jurisdictional claims in published maps and institutional affiliations.

Copyright: © 2022 by the authors. Licensee MDPI, Basel, Switzerland. This article is an open access article distributed under the terms and conditions of the Creative Commons Attribution (CC BY) license (https://creativecommons.org/licenses/by/4.0/).

1. Introduction

The Intergovernmental Panel on Climate Change (IPCC) 2021 has indicated that global temperatures increased by nearly 1.1 °C in the period from 1850 to 2000; it was found that global mean temperature is expected to increase by 1.5 °C or more over the next two decades relative to these values. The cryosphere, one of the sensitive areas for climate

change, is facing increasing challenges. Moreover, the global warming effect is magnified at high latitudes and altitudes and exerts significant effects [1–3]. The permafrost has also changed significantly with global warming. Heilongjiang Province, the main high-latitude permafrost distribution area in China, belongs to the southern edge of the permafrost zone in eastern Eurasia [4]; its permafrost is largely distributed in the Daxing'an mountain region in the north, with predominantly seasonal frozen ground in the south [4,5]. Due to the unique hydrothermal properties of permafrost, different types of permafrost have different effects on the construction of roads, bridges and oil pipelines in cold regions, as well as on agricultural production.

Since the 1950s, permafrost research in northeastern China has aroused considerable attention [6]. However, due to the lack of long-term actual measurement data, the research on permafrost in the north-east is currently dependent on major projects (e.g., geological surveys, highways and Russian–Chinese oil pipelines). Such research has been mostly performed through borehole monitoring. Wang [7] investigated the effect of an oil pipeline on the surrounding permafrost and the mitigation effect of the installed thermosiphon on the degradation thereof, based on the ground temperature monitoring data from two sections of the Russian–Chinese oil pipeline (Jiagedaqi section) from 2011 to 2017. Li [8] studied the distribution of permafrost at four representative stations along the Russian–Chinese Crude Oil Pipelines 1 and 2 through resistivity tomography. It was revealed that the construction of the pipelines affects permafrost in permafrost areas more significantly than in seasonal frozen ground areas. Dong [9] monitored the soil temperature and moisture in the scrub and forest in the Daxing'an mountain region. He drew the conclusion that the freeze–thaw process in the active layer exhibits two-way freezing and one-way melting, with the melting time being greater than the freezing time. This result suggested that the mean annual soil temperature in the forest is greater than that in the scrub at the same depth, while the annual mean water content is less than that in the scrub. Li [10] explored the effects of forest fires on the thermal state of near-surface permafrost and the active layers in two forest fire zones (Mangui and Longshan) at the northern foot of the Daxing'an mountains in northeast China. Post-fire ground temperature increases with the increase of the fire severity and primarily occurs at depths of 0~1.5 m, as indicated by the results. The same authors [11] monitored the active layer and permafrost temperatures at four monitoring sites with different surface characteristics in the Nanweng River wetland in the Daxing'an mountain region from 2012 to 2019. The research revealed that the active layer at the monitoring sites in the permafrost zone becomes thinner, and the depth of the active layer at the monitoring sites in the seasonal frozen ground zone is more sensitive to climate warming.

However, point-line data from boreholes cannot fully indicate the spatial variability of permafrost or quantify the spatial–temporal variability thereof. As such, freezing/thawing indices and reanalysis data have been introduced in analyses of the spatial–temporal distribution of large areas of permafrost [12,13]. These indices have been confirmed as a vital factor for evaluating climate change, cryosphere changes, hydrological and ecological processes and engineering stability in cold regions [14–17]. The atmospheric freezing/thawing index and the ground freezing/thawing index are two common indices [18]. Since near-surface air temperatures represent a complex energy balance between the ground (summer vegetation layer and winter snow) and the atmosphere [19], surface temperatures examined at 0–5 cm are more correlated with the thermal state of permafrost and reveal the heat balance between the ground and the atmosphere [13], thus taking on critical significance to the freezing process of permafrost [20]. However, most weather stations lack surface temperature observations, and freezing/thawing indexes calculated from air temperature have been employed in many cases for permafrost research. In addition, the N factor for the ratio of the near-surface air freezing/thawing index to the ground freezing/thawing index has been increasingly adopted to determine the ground freezing/thawing index [18,21–23]. The use of reanalyzed grid air temperature data to calculate freezing/thawing indices has also been widely used in permafrost areas [14,21,24–27]. Wu [28] analyzed the

spatial–temporal trends of the freezing/thawing index of 20 meteorological stations in Mongolia and noted that 70% of the stations showed an increasing trend. Frauenfeld [14] found that climatology based on long-term changes in freezing/thawing indices in cold regions is closely correlated with seasonal temperature changes. In perennial permafrost zones, the freeze–thaw process in the active layer is closely correlated with changes in the thawing index and temperature [27,29,30]. The latest findings indicate a decreasing/increasing trend in the freezing/thawing index in the northern hemisphere permafrost zone since 1901, with significant changes in the freezing/thawing index in the circumpolar arctic permafrost zone after 1988 [26]. Zhang [19] used weather station and CMFD data from 1980–2010 to analyze climate change and the changes in permafrost distribution under its influence in the north-eastern region. Using MODIS LST data, Shan [31] determined that permafrost change in the northeast is characterized by a northward shift of the southern edge, a shrinking of the associated island and a decrease in stability at the edge. Shan [32] used the MODIS Terra/Aqua product to simulate a reduction in the area of permafrost from 32.77×10^4 km^2 to 27.10×10^4 km^2 in the northeast from 2003–2019 by establishing a numerical correlation between the ground freezing/thawing index of permafrost and the MAGST. Using 11 CMIP6 global climate models, Xu [33] simulated a significant decreasing trend in surface temperature and a slight decreasing trend in the permafrost zone in Heilongjiang Province from 1960–2014. The permafrost zone is predicted to shrink significantly from 2015–2100. Song [34] analyzed the spatial distribution of key variables in the soil freeze–thaw process using surface temperature data monitored from 34 meteorological stations in Heilongjiang Province, and discussed the spatial–temporal distribution of key variables and changes in surface temperature in the freeze–thaw process under different vegetation types. Accordingly, the freezing/thawing index can be employed to map the distribution of permafrost and is of great significance for the evaluation of changes in the distribution of permafrost and its contribution to climate. Briefly, under the combined effect of regional geological conditions, climate warming and human activities [35], the MAAT in northeast China has increased at 0.6 °C/10a over the past 30 years and 0.72 °C/10a over the past 10 years; this rate of increase is higher than the global mean [36–38]. As a result, the permafrost in the north-east is also gradually degrading [39–43]. From the 1950s to the 2010s, the southern boundary of the permafrost shifted north by 0.1 to 1.1° [44]. However, most of the current research on permafrost in the northeast is focused on the perennial permafrost in the Daxing'an mountain region and has mostly been carried out using data from monitoring points on existing infrastructure, such as the Russian–Chinese oil pipeline and the Jiamo Highway. For environmental reasons, monitoring points are sparse, and the monitoring time and extent is limited, such that spatial–temporal analyses with long series and covering large areas are difficult to conduct. Due to the difficulty of monitoring surface temperatures, most existing studies on freezing/thawing indices use air temperature data for relevant analyses; however, such data do not fully represent the changes in the thermal state of the surface, and there is a certain error in the research on permafrost distribution.

Therefore, this study takes Heilongjiang Province as its study area and uses daily surface temperature data from 1971 to 2020 for the following purposes: (1) to analyze the spatial–temporal distribution characteristics of MAAT, MAGST, the mean annual AFI, ATI, GFI and GTI; and (2) to explore the permafrost trends in Heilongjiang Province based on a surface freezing index model from 1971 to 2019. The above research results are critical to the analysis of the trend of permafrost degradation in Heilongjiang Province and the effect of climate on permafrost under climate warming, as well as to the mapping of the distribution of large areas of permafrost using the surface freezing index model. Thus, this study can provide a reference for natural cold resource development, ecological protection, climate change and engineering construction and maintenance in permafrost areas.

2. Data and Methods

2.1. Study Area

Northeast China is the main high-latitude permafrost distribution area in China and one of the most sensitive regions to climate warming [45]. Heilongjiang Province is located in the northern part of the Northeast (121°11′ E–135°05′ E, 43°26′ N–53°33′ N) and is bordered by Russia in the north, Inner Mongolia and Jilin Provinces in the west and south respectively, and the Sea of Japan in the east. The main mountain ranges in the territory are the Daxing'an and Xiaoxing'an Mountains in the north, the Zhang Guang'cai Mountains, the Laoyeling and the Wanda Mountains in the southeast, with the Songnen Plain and the Sanjiang Plain on either side. The main rivers are the Heilongjiang, Songhua, Nenjiang and Suifen rivers. The climate is largely a cold-temperate and temperate continental monsoon climate with cold and long winters and short summers [46]. The MAAT ranges between −4 and 5 °C and the total mean annual precipitation is 400–600 mm [33], with rich forestry and agricultural resources [47,48].

2.2. Data Sources

The meteorological data used in this study were obtained from the National Meteorological Science Data Centre of China (http://data.cma.cn/, accessed on 28 July 2022) for the period 1971–2020 for 34 stations in Heilongjiang Province, including daily mean air temperature and daily mean ground temperature. The remote sensing data were reanalyzed using the "ERA5-Land monthly averaged data from 1981 to present" (https://doi.org/10.24381/cds.68d2bb30, accessed on 15 August 2022) with a spatial resolution of 0.1° × 0.1°. The distribution of meteorological stations is shown in Figure 1. The digital elevation data (DEM) of Heilongjiang Province were obtained from a digital surface model with a 30 m spatial resolution, provided by the Japan Aerospace Exploration Agency (JAXA). The air temperature and ground surface temperature data are generally complete, but there are still some missing measurements, which are interpolated using the following methods.

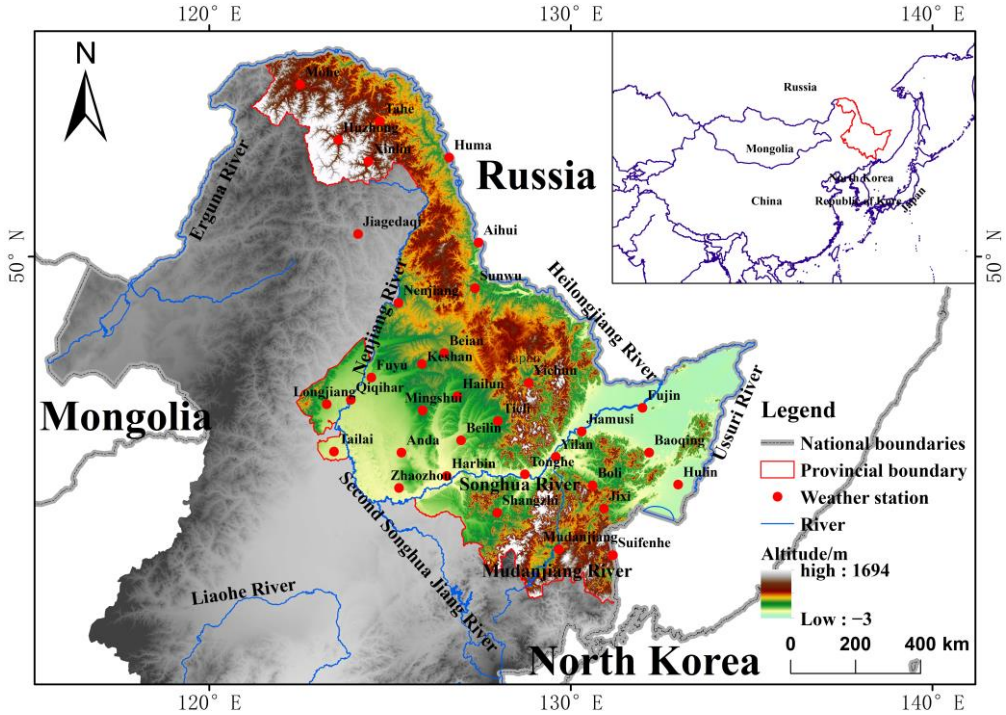


Figure 1. Study area and distribution of meteorological stations.

1. A single day of missing measurement: interpolate the missing data with the mean of the data for the days before and after the day of missing measurement.
2. Two consecutive days of missing measurements: the means of the data for the two days before the first day of missing measurements and of the data for the two days after the second day of missing measurements are interpolated.
3. Missing measurements for more than two consecutive days: The double cumulative curve method is often used to check the consistency of hydro-meteorological elements and to interpolate missing values or to correct information.

Due to the impact on the trend of surface temperature change resulting from the change in the monitoring method of surface temperature data at the site after 2004, the double cumulative curve method was used to correct the daily ground temperature data based on the trend of temperature at the respective station, and the corrected data were verified using the monthly averaged remote sensing data for the same period. The correlation between the monitored surface temperature and the remotely sensed inversion surface temperature at sites in the periods of 1981–2004, 2005–2019 and 1981–2019 before correction are depicted in Figure 2a–c, with R^2 of 0.995, 0.954 and 0.962, respectively. Figure 2d shows the correlation between the monitored surface temperature in the period of 1981–2019 after correction, as well as the correlation between the monitored surface temperature and the remotely sensed inversion surface temperature in the period of 1981–2019 after correction, with R^2 of 0.991, all of which passed the significance test. It can be concluded that the correlation between the corrected surface temperature data and those obtained from the remotely sensed inversion is high and can meet the needs of the present analysis.

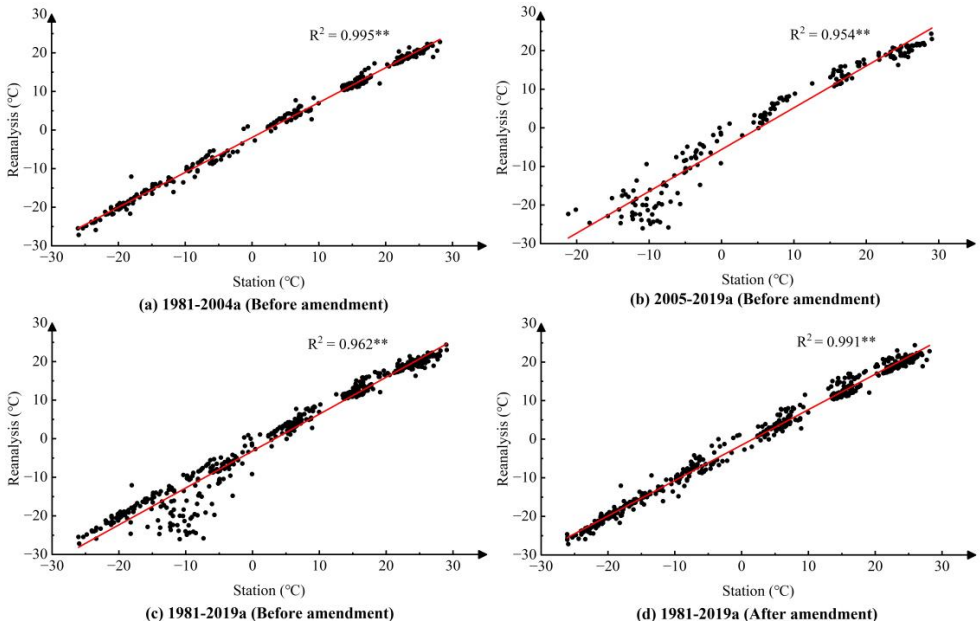


Figure 2. Validation of MODIS month-by-month ground surface temperature against weather station month-by-month ground surface temperature (** indicates reaching the significance level of $\alpha = 0.01$).

2.3. Research Methods

2.3.1. Computation of the Freezing/Thawing Index

The freezing/thawing index comprises the freezing index and the thawing index; it refers to the sum of all temperatures less than and greater than 0 °C throughout the freezing and thawing periods, respectively. To ensure the continuity of the calculation, the freezing period was defined in this study as the period from 1 July to 30 June of the

following year, and the thawing period was defined from 1 January to 31 December [49,50]. The freezing/thawing index is expressed as follows [14,15,26,28].

$$FI = \sum_{i=1}^{N_F} |T_i|,\ T_i < 0 \quad (1)$$

$$TI = \sum_{i=1}^{N_T} |T_i|,\ T_i > 0 \quad (2)$$

where *FI* denotes the annual freezing index (°C·d), including the annual AFI and GFI; *TI* represents the annual thawing index (°C·d), including the annual ATI and GTI; T_i expresses the mean daily temperature during the freezing period, i = 1, 2, 3 … … N_F, with N_F as the number of days during the freezing period when the temperature is less than 0 °C; and T_i represents the daily mean temperature in the thawing period, i = 1, 2, 3 … … N_T, with N_T as the number of days during the thawing period when the temperature is higher than 0 °C.

2.3.2. Surface Freezing Index Model

GFI and GTI were adopted to delineate the boundary between permafrost and seasonal frozen ground [18].

$$\mathrm{F} = \frac{\sqrt{\mathrm{GFI}}}{\sqrt{\mathrm{GFI}} + E + \sqrt{\mathrm{GTI}}} \quad (3)$$

where F denotes a parameter to evaluate the presence or absence of permafrost and to distinguish the type of permafrost, and *E* is an empirical value for estimating the condition of permafrost. This study combines the empirical value range of 0.5–1.5 and a common value of *E*, i.e., 1. F = 0.5 is defined as the threshold value for the presence or absence of permafrost; F < 0.5 means seasonal frozen ground while F > 0.5 means permafrost [26].

2.3.3. Analysis Methods

A linear trend fit was used to analyze interannual trends in MAAT, MAGST, FI and TI [48,51], and a local thin-disk smooth spline function interpolation method was chosen for the spatial analysis to interpolate MAAT, MAGST, FI and TI from the point scale to the regional scale [52]. Pearson's correlation coefficient was deployed to examine the correlation between the freezing/thawing index and MAAT.

3. Results

3.1. Spatial and Temporal Characteristics of MAAT and MAGST

Figure 3 shows the interannual variation and spacing trends of MAAT and MAGST in Heilongjiang Province from 1971–2019. From Figure 3a,b, it can be seen that both MAAT and MAGST show an increasing trend, the trends are relatively consistent and both pass the 99% significance test, but the trend of MAAT is more pronounced than that of MAGST. The multiyear range of variation in MAAT is 0.87–3.83 °C, with a warming rate of 0.34 °C/10a, and the multiyear range of variation in MAGST is 2.25–5.75 °C, with a warming rate of 0.33 °C/10a. The range of variation in MAGST is higher than that of MAAT, and conversely, the rate of variation in MAAT is higher than that of MAGST. The main reason for the inconsistency in warming trends is that factors affecting surface temperature are correlated with vegetation type, snow cover and geological conditions as well as air temperature [33,53,54]. Additionally, the effect of different types of mulch on surface temperature also varies [34]. As can be seen in Figure 3b, the variation in temperature is also inconsistent over time, with MAAT remaining largely below the 49a multiyear mean until 1987, indicating a cooler period, while from 1988 to 2019, the MAAT were mostly greater than the multiyear mean, indicating a distinctly warmer period. This trend also confirms the trend of increasing air temperatures and surface temperatures year by year. In addition, from 1971–2019, the MAAT was lower than the MAGST, with a positive temperature difference between air and ground. Besides the facts that the warming effect of the atmosphere is greater than the cooling effect and that heat transfer from the

surface to the atmosphere is dominant in Heilongjiang Province, it may also be correlated with the thermal effect of surface coverage, which affects the seasonal distribution patterns of air and surface temperatures [49]. Previous studies at high latitudes have shown that the thermal effect of snow cover in winter is usually greater than that of vegetation cover in summer, and that in most cases, the MAAT is greater than the MAGST [55]. The results of the study are consistent with trends in air and surface temperatures in other parts of the country [56,57].

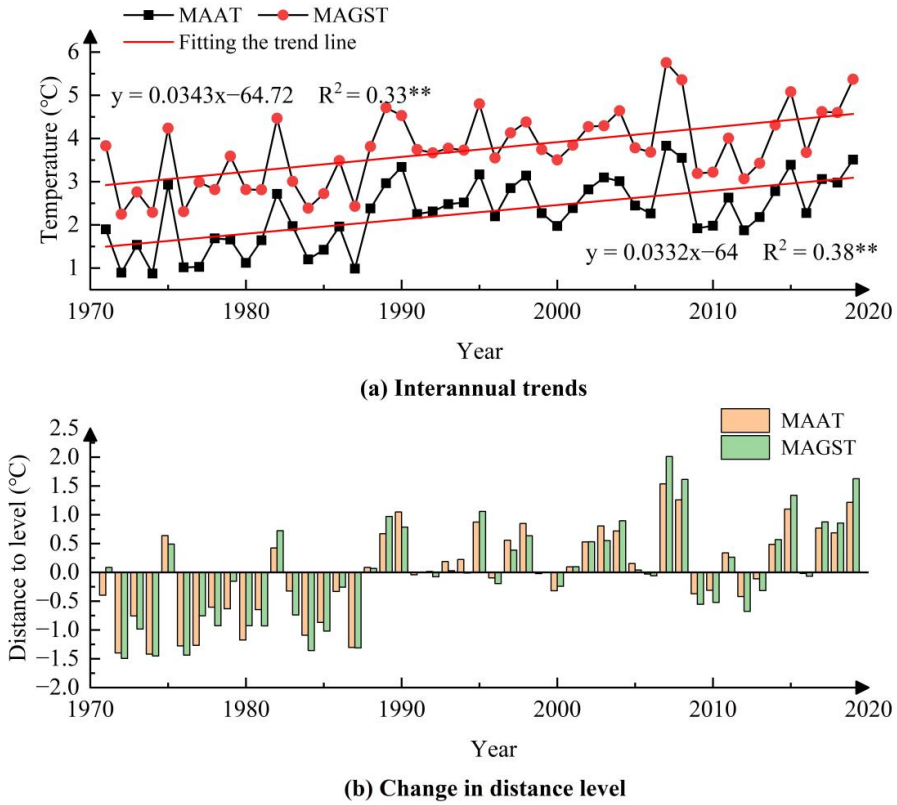


Figure 3. Interannual and distance-level trends in MAAT and MAGST in Heilongjiang Province from 1971 to 2019 (** indicates reaching the significance level of $\alpha = 0.01$).

Figure 4 presents the spatial distribution of MAAT and MAGST in Heilongjiang Province from 1971–2019. As depicted in Figure 4a, the variation of MAAT showed a clear latitudinal trend: the higher the latitude, the lower the MAAT. Furthermore, the variation of multiyear MAAT ranged from −8.64 to 5.60 °C throughout Heilongjiang Province. At the same latitude, the change in MAAT also showed a trend, i.e., the higher the altitude, the lower the MAAT. For instance, in the Daxing'an mountain region in the north, from right to left, the MAAT tended to decrease with the increase of altitude, and the province's MAAT also occurred in the Daxing'an Mountains. In the southern region, with the Xiaoxing'an and Zhangguang'cai mountains ranges as the dividing line, toward the Songnen Plain (left) and the Sanjiang Plain (right) on either side, the MAAT gradually increases as the altitude decreases. As depicted in Figure 4b, the spatial variation of MAGST also showed a latitudinal trend from south to north. With the increase of latitude, the MAGST tended to decrease, and the variation of multiyear MAGST throughout Heilongjiang Province ranged from −6.52 to 7.58 °C. The minimum and maximum MAGST were both higher than the MAAT. However, both the 0 °C isotherm and the minimum temperature of the MAGST occurred further north than the MAAT. The 0 °C isotherm of the multiyear MAAT in Heilongjiang Province was affected by altitude and was more scattered between 45° and 51° N; the 0 °C isotherm of the multiyear MAGST was between 50° and 51° N. The critical reason for the difference in the spatial distribution of MAAT and MAGST is the difference

in heat exchange between the atmosphere and the surface due to the balance of energy at the surface [58–61]. Additionally, ground cover (e.g., vegetation and snow) is a critical factor for heat exchange [62,63]. Vegetation affects surface temperature mostly by isolating the soil from the atmosphere, thus reducing wind speed near the surface. As a result, the evaporation of water from the surface soil layer was reduced, and heat was released into the atmosphere [64–66], while vegetation also attenuated most of the solar radiation and directly reduced the surface temperature [67,68]. Additionally, different vegetation types have different effects on soil moisture evaporation and solar radiation [64,69]. The effect of snow on surface temperature is twofold: during the freezing period, snow and vegetation have the same effect, isolating the soil from the atmosphere, reducing the effect of cold air and wind speed on ground temperature and insulating the soil at the surface. During the melting period, melting snow will absorb heat from the surface soil, thus reducing surface temperature [70,71].

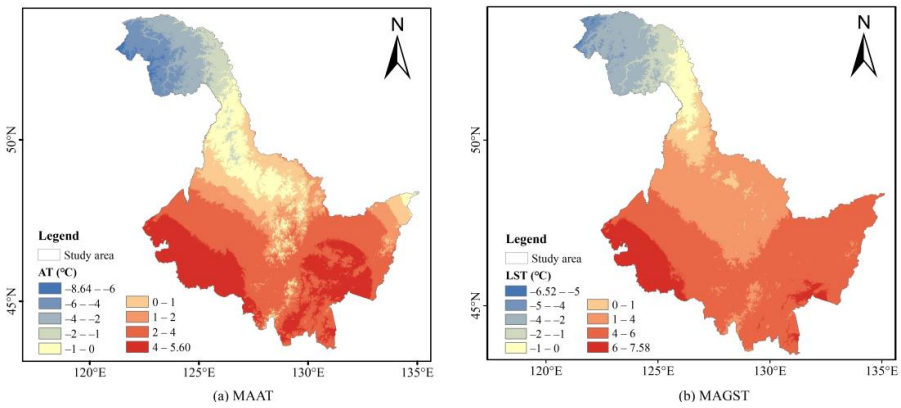


Figure 4. Spatial variation of MAAT and MAGST in Heilongjiang Province.

3.2. Temporal Variation Characteristics of the Freezing/Thawing Index

Figure 5 presents the temporal variation characteristics of the freezing/thawing index in Heilongjiang Province. Both the mean annual AFI and GFI for Heilongjiang Province for the 1971–2019 period show an overall decreasing trend. The former ranged from 1630.84 to 2714.01 °C·d, with a decreasing trend of −5.07 °C·d·a^{-1}, with a minimum in 2018 (1630.84 °C·d) and a maximum in 1976 (2714.01 °C·d). The multiyear range of the mean annual GFI was 1703.84–2795.65 °C·d, with a downward trend of −5.04 °C·d·a^{-1}, with a minimum in 2018 (1703.84 °C·d) and a maximum in 1976 (2795.65 °C·d), which is consistent with the trend in the mean annual AFI. There was an overall upward trend in the mean annual ATI and GTI, with the multiyear variation range of the mean annual ATI being 2827.32–3375.42 °C·d and its upward trend being 7.63 °C·d·a^{-1}, with the highest being in 2018 (3375.42 °C·d) and the lowest in 1972 (2827.32 °C·d). The mean annual GTI varied from 3229.21 to 4043.12 °C·d, with an upward trend of 11.89 °C·d·a^{-1}, with a maximum in 2014 (4043.12 °C·d) and a minimum in 1972 (3229.21 °C·d). For the range of variability, the maximum and minimum values of the interannual range of the air/ground freezing/thawing index were significantly smaller in Heilongjiang Province than in the Yakutia region of Russia due to latitude and altitude [72] and larger than in the Heilongjiang basin [16]. The mean annual AFI over the study period was also larger than in Russia, Alaska and Canada for 1901–2015, and the mean annual ATI was smaller than in Russia and Canada and larger than in Alaska [26].

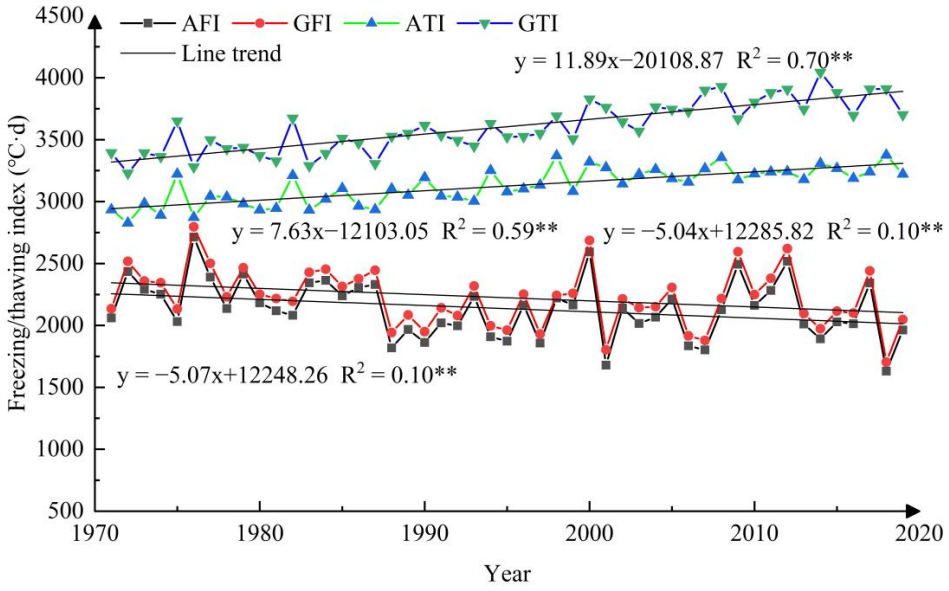


Figure 5. Interannual trends in air/ground freezing/thawing index in Heilongjiang Province from 1971 to 2019 (** indicates reaching the significance level of $\alpha = 0.01$).

By calculating the distance level of the freezing/thawing index in Heilongjiang Province (Figure 6), the temporal change characteristics of that index can be more intuitively understood. The overall decreasing trend of the mean annual AFI and GFI from 1971 to 2019 is the same, and the decreasing rates of both are very similar. Conversely, the increasing trends of the mean annual ATI and GTI are also the same, but the increasing rate of the mean annual GTI is faster than that of the mean annual ATI. For rate of change, the rate of decline in the air/ground FI in Heilongjiang Province is significantly smaller than that in the Qinghai-Tibet Plateau and Mongolia (1961–2011) [73] and in northeastern China as a whole (1972–2005) [49]. Additionally, the rising trend in the air/ground TI is smaller than that in the northeast, except for all other regions. The difference in the variable interannual trends of the freezing/thawing index suggests that the degree of permafrost degradation is faster in Heilongjiang Province than in the Qinghai-Tibet Plateau and Mongolia and is also the fastest in the northeast. However, the same calculation methods and uniform time series should be adopted to compare the changes in the freezing/thawing indices in different regions.

3.3. Spatial Variation Characteristics of the Freezing/Thawing Index

The spatial distribution characteristics of the mean annual FI in Heilongjiang Province from 1971 to 2019a are shown in Figure 7a,c, with the variation range of the mean annual AFI being 1385.64–4271.13 °C·d and that of the mean annual GFI being 1466.07–4464.10 °C·d. Additionally, the minimum and maximum values are higher than the mean annual AFI, primarily because the MAGST is higher than the MAAT in Heilongjiang Province due to the effect of ground cover. For spatial distribution, both the mean annual AFI and the mean annual GFI show a latitudinal trend, especially in the southern region. For example, in Fuyuan, the easternmost city in Heilongjiang Province, located in the Three Rivers Plain, the mean annual AFI is higher than in other areas of the Three Rivers Plain, despite the low altitude. However, the latitude is relatively higher than in other areas of the Plain. This result is consistent with those of studies that have found the existence of permafrost in the Fuyuan area [5,74]. In addition, in the northern Daxing'an mountain region, the effect of altitude on the AFI and GFI is more pronounced, showing a trend of increasing air/ground FI from right to left according to altitude.

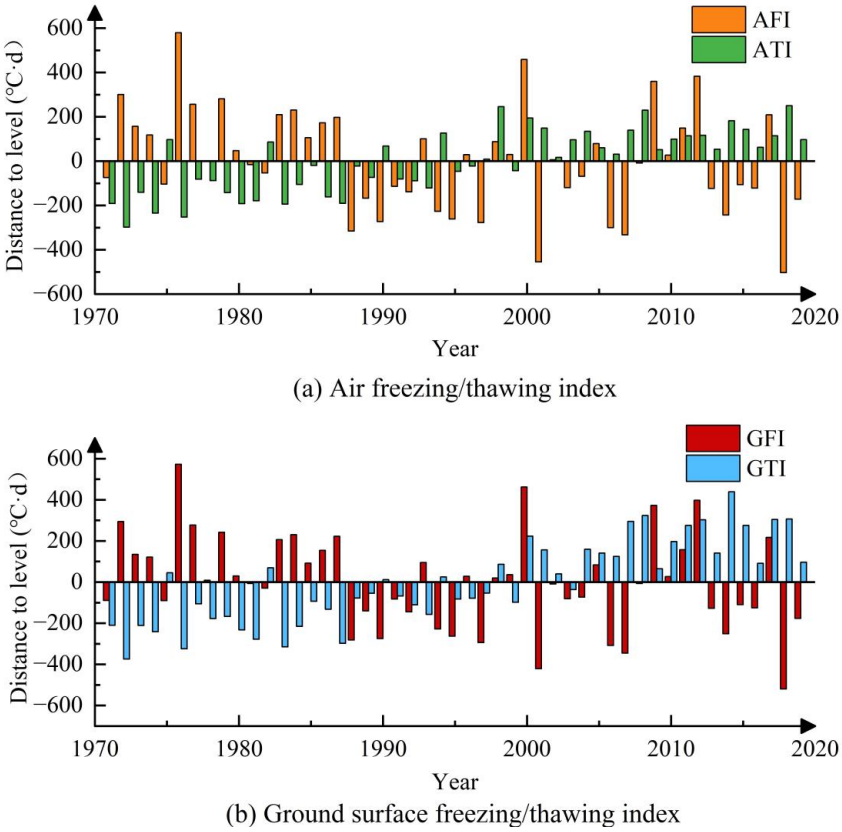


Figure 6. Variation of air/ground freezing/thawing index distance level in Heilongjiang Province from 1971 to 2019.

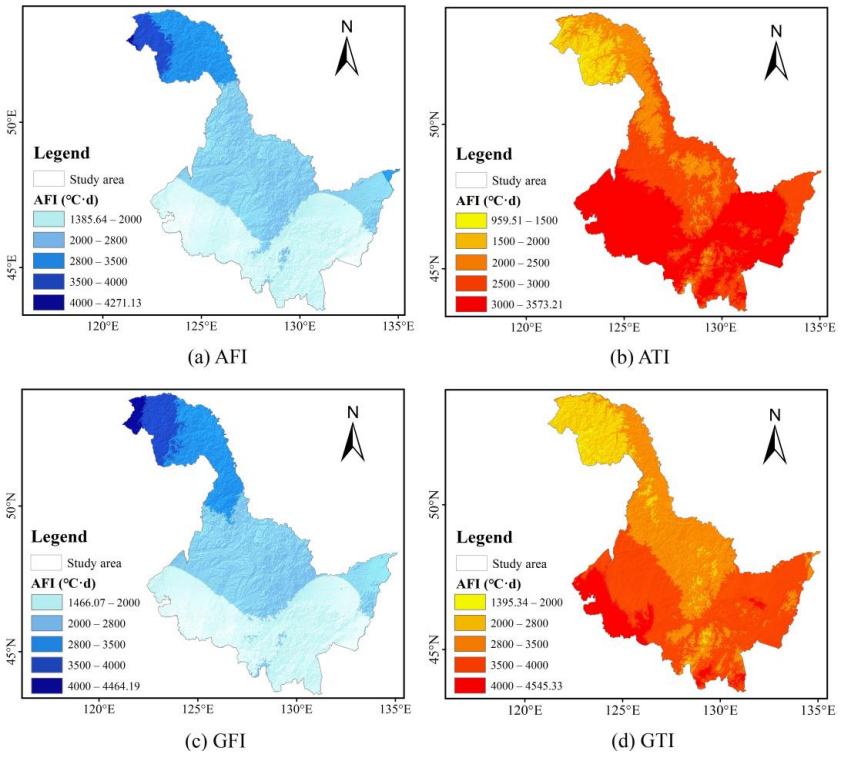


Figure 7. Spatial trends in air/ground freezing/thawing index in Heilongjiang Province.

The spatial distribution characteristics of the mean annual TI in Heilongjiang Province from 1971 to 2019a are shown in Figure 7b,d, with the variation range of the mean annual ATI being 959.51–3573.21 °C·d and the variation range of the mean annual GTI being 1395.34–4545.33 °C·d. The minimum values of both the mean annual ATI and GTI occur in the Daxing'an mountain region in the north, and the maximum values of the mean annual ATI and GTI occur in the Songnen and Sanjiang plains. In spatial distribution, both show the same latitudinal trend, especially in the south, where altitude plays a major role in the distribution of the mean annual air/ground TI. The difference is that the mean annual ATI > 2000 °C·d is distributed over a larger area than the mean annual GTI, and the mean annual GTI distribution is more discrete in the southern mountainous regions, where the effect of altitude is more pronounced.

The rates of change of the mean annual air/ground freezing/thawing index at the various stations in Heilongjiang Province from 1971 to 2019 are shown in Figure 8. From Figure 8a, it can be seen that the rate of decline of the mean annual AFI ranged from −13.92 to −136.36 °C·d/10a, with the largest rate of decline at Sunwu station (−136.36 °C·d/10a), which passed the 0.01 significance test. Meanwhile, the rate of decline at Tailai station was the smallest (−13.92 °C·d/10a), did not pass the significance test and the declining trend was not obvious. Notably, 13 out of 34 stations, mostly in the Sanjiang Plain and the Songnen Plain, did not pass the 0.05 significance test. The rate of decrease of the mean annual GFI is shown in Figure 8c; it varies from −8.30 to −180.95 °C·d/10a, and like the mean annual AFI, the maximum and minimum rates of decrease are at Sunwu station (−8.30 °C·d/10a, which passed the significance test of 0.01), and Tai Lai station (−180.95 °C·d/10a, which did not pass the significance test of 0.05). The spatial rate of change of the mean annual GFI for the whole Heilongjiang Province did not pass the significance test at 17 out of 34 stations, with similar distribution characteristics as the mean annual AFI.

The distribution of the rising rates of air/ground TI for the various stations in Heilongjiang Province from 1971 to 2019 are presented in Figure 8b,d, both of which passed the significance test of 0.05. The range of variation in the rate of increase of the mean annual ATI reached 20.37–126.57 °C·d/10a, with Sunwu (126.57 °C·d/10a) being the fastest rising station and Mohe (20.37 °C·d/10a) the slowest. The rate of increase of the mean annual GTI ranged from 49.23 to 171.43 °C·d/10a, with Sunwu (171.43 °C·d/10a) being the fastest rising station and Mohe (49.23 °C·d/10a) the slowest. However, both showed faster rates of increase than the mean annual ATI. This finding also demonstrates that the most pronounced warming in NE China over the last few decades has been at Sunwu [37].

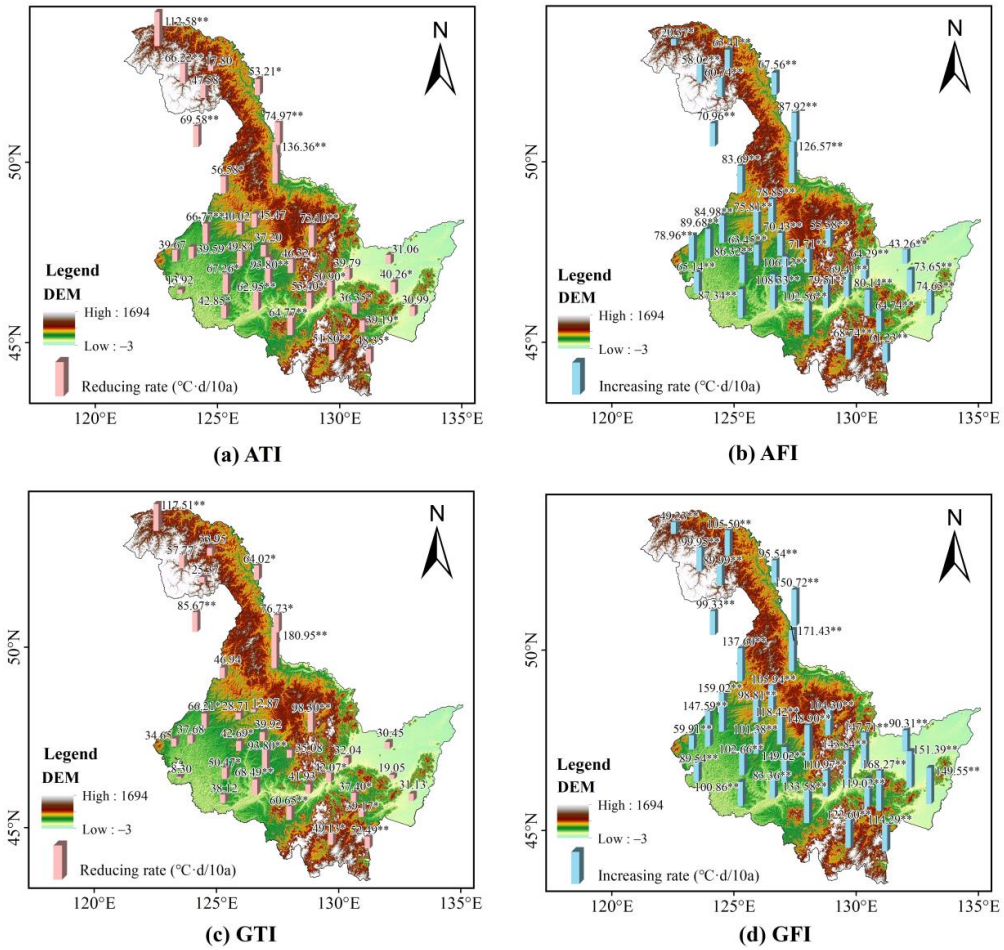


Figure 8. Spatial rate of change of air/ground freezing/thawing index in Heilongjiang Province (** indicates reaching the significance level of $\alpha = 0.01$). * indicates reaching the significance level of $\alpha = 0.05$.

4. Discussions

4.1. Correlation between Freezing/Thawing Index and MAAT

In general, the MAAT in Heilongjiang Province showed a significant negative linear correlation with the air/ground FI, with both passing the 0.01 significance tests, as shown in Figure 9a,b. A comparison of the linear correlation between the mean annual AFI and GFI and the MAAT indicated that the linear correlation between the mean annual AFI and GFI and the MAAT is almost identical. With the increase of the temperature, the mean annual GFI decrease at 185.14 °C·d/°C and the mean annual AFI decrease at 184.36 °C·d/°C, the difference was not significant. The main reason for this result is the warming and wetting of the freezing period in Heilongjiang Province due to rising temperatures and the winter burning wind effect, thus reducing the depth of the snowpack. As a result, the snowpack became less effective at insulating ground temperatures, which are more sensitive to temperature changes [75,76]. The air/ground TI showed a significant positive linear correlation with the MAAT, with both passing the 0.01 significance test, as shown in Figure 9c,d. Comparing the correlation between the mean annual ATI and GTI with the MAAT revealed that the linear correlation between the mean annual ATI and the MAAT is better than that of the mean annual GTI as the temperature increases. This is because both the MAAT and the mean annual AFI are calculated from the mean daily air temperature, and the mean annual GFI was determined from the mean daily ground temperature. Furthermore, there was a lag in the response of surface temperature to air temperature under the effect of cover (e.g., snow and vegetation) [13,77]. The rate of change of the mean annual GTI with the increase of the air temperature was 176.71 °C·d/°C, higher

than the rate of change of the mean annual ATI of 135.17 °C·d/°C. The above result was consistent with previous findings, i.e., that the increasing trend of the mean annual GTI was greater than that of the mean annual ATI.

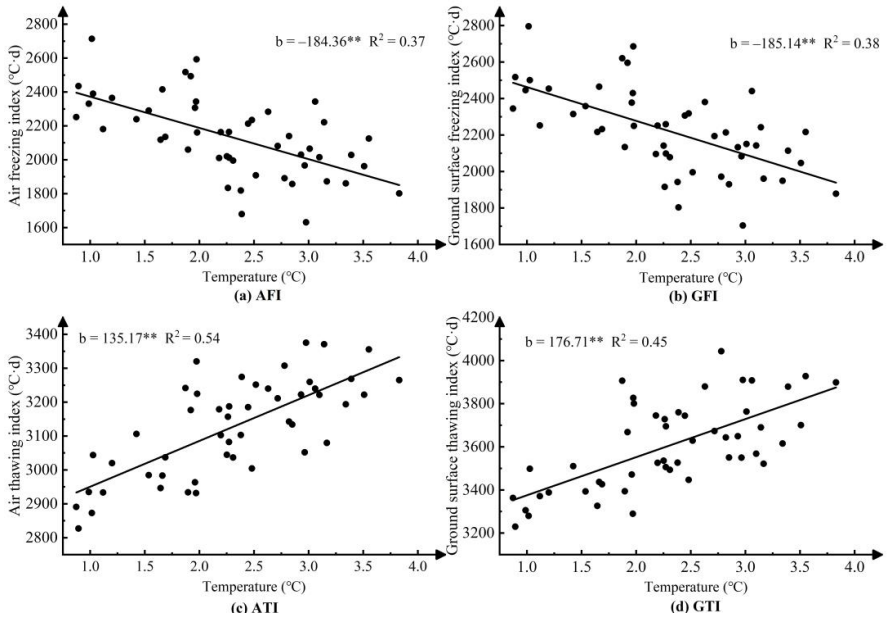


Figure 9. Correlation between MAAT and air/ground freezing/thawing index (** indicates reaching the significance level of $\alpha = 0.01$).

4.2. Changes in the Distribution of Frozen Soil Based on the Surface Freezing Index Model

Figure 10 presents the spatial–temporal distribution of permafrost and seasonal frozen ground in Heilongjiang Province obtained based on the surface freezing index model for the 1971–2019 period. Permafrost is largely distributed in the Daxing'an and Xiaoxing'an Mountains in the north and sporadically in several mountainous areas in the central part of the province. The southern permafrost boundary has shifted nearly 2° to the north since the 1970s, and the total area of permafrost shrank from 1.11×10^5 km^2 in the 1970s to 6.53×10^4 km^2 in the 2010s (Table 1), a decrease of nearly 40.9%, with a significant trend of permafrost degradation. The overall trend of change is also consistent with the change in the southern boundary of the permafrost across northeast China [78]. From the 1970s to the 1980s (Figure 10a,b), the trend of northward shift of the southern boundary of permafrost was not obvious, and permafrost degradation was mostly manifested by the gradual degradation of a large area of discontinuous permafrost between 46 and 48° N to island permafrost or seasonal frozen ground. In contrast, from the 1980s to the 1990s (Figure 10b,c), the northern shift of the southern permafrost boundary was obvious, with a shift of nearly 1.5° N, except for discontinuous and island permafrost which almost entirely degraded to seasonal frozen ground, and permafrost in the eastern part of Huma, which also gradually degraded to seasonal frozen ground. From the 1990s to the 2000s and 2010s (Figure 10c–e), the trend of permafrost degradation in the north–south direction slowed, with the southern boundary of permafrost remaining basically at around 51° N. Permafrost degradation was manifested as a gradual degradation of permafrost to seasonal frozen ground at lower elevations in the east between 51° and 53° N. The trend of degradation showed a progressive degradation of permafrost from right to left with the increase of the elevation and over time, confirming the suspected severe permafrost degradation in the Huma region [31]. Besides the differences in permafrost degradation in different decades, which are correlated with the changes in MAAT and MAGST over the previously analyzed periods, the insulating effect of snowpack can lead to an increase in ground temperature, resulting in a thinning of the active layer and permafrost degradation [6,71]. Furthermore, external factors (e.g., vegetation, forest fires and urbanization [78–80]), as well as internal

factors (e.g., geological conditions and the water content of the shallow ground surface) can affect the degradation of permafrost [6,81].

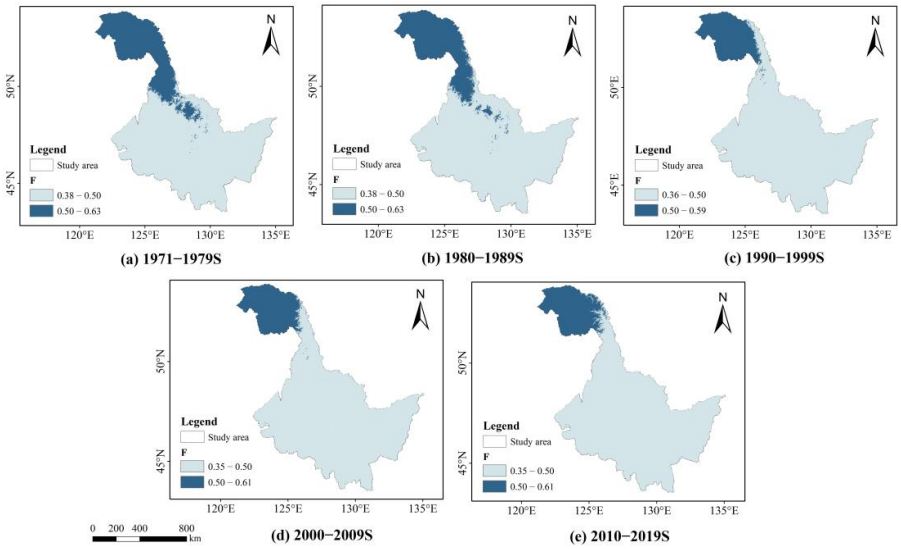


Figure 10. Interdecadal distribution of permafrost and seasonal frozen ground in Heilongjiang Province from 1971 to 2019 ($0.5 \leq F < 1$: indicates permafrost, $0 \leq F < 0.5$: indicates seasonal frozen ground).

Table 1. Area of permafrost and seasonal frozen ground in different interdecadal periods in Heilongjiang Province from 1971 to 2019.

Period	Permafrost		Seasonal Frozen Ground	
	Area/km^2	Proportion	Area/km^2	Proportion
1971–1979s	110,541	24.26%	345,073	75.74%
1980–1989s	101,046	22.18%	354,568	77.82%
1990–1999s	66,186	14.53%	389,428	85.47%
2000–2009s	65,779	14.44%	389,835	85.56%
2010–2019s	65,333	14.34%	390,281	85.66%

5. Conclusions

In this study, based on the mean daily air temperature and mean daily ground temperature data from 34 meteorological stations in Heilongjiang Province from 1971 to 2019, the air/ground freezing/thawing indices were determined. Additionally, the spatial–temporal variation characteristics of the MAAT, MAGST and mean annual air/ground freezing/thawing index in Heilongjiang Province were studied, and the correlation between the MAAT and the mean annual air/ground freezing/thawing index was analyzed. Furthermore, the trends in the distribution of permafrost in Heilongjiang Province were explored based on the surface freezing index model. The main conclusions are as follows.

1. The spatial distribution of MAAT and MAGST in Heilongjiang Province shows a decreasing trend with the increase of the latitude and altitude; the MAAT in Heilongjiang Province is higher than the MAGST, and they all tend to be on an upward trend, with a range of −8.64–5.60 °C for the multiyear MAAT and of −6.52–7.58 °C for the multiyear MAGST.
2. During the study period, the mean annual AFI and GFI showed a decreasing trend, and the decreasing trend of both was almost the same. The mean annual ATI and GTI both showed an overall increasing trend, and the increasing trend of the mean annual GTI was greater than that of the mean annual ATI, with an increasing rate of 7.63 °C·d·a^{-1} and 11.89 °C·d·a^{-1}, respectively.

3. For spatial distribution, the mean annual air/ground freezing/thawing index also showed a latitudinal trend, but in the northern Daxing'an mountain region, altitude plays a major role in the distribution of freezing/thawing index, while latitude has a greater influence on the distribution of freezing/thawing index than altitude in the southern region. Across Heilongjiang Province, the range of variation of the mean annual AFI was 1385.64–4271.13 °C·d, the range of variation of mean annual GFI was 1466.07–4464.10 °C·d, the range of variation of the mean annual ATI was 959.51–3573.21 °C·d and the range of variation of the mean annual GTI was 1395.34–4545.33 °C·d.
4. Permafrost in Heilongjiang Province is primarily distributed in the northern Daxing'an Mountains and Xiaoxing'an Mountains and sporadically in some mountainous areas in the central part of the province. For the 1970–2010 period, the trend of permafrost degradation is obvious; the southern permafrost boundary moved nearly 2° to the north and the total permafrost area shrank from 1.11×10^5 km^2 in the 1970s to 6.53×10^4 km^2 in the 2010s, a reduction of approximately 40.9%. The southern boundary of permafrost in the 2010s was nearly stable at around 51° N.

Author Contributions: Conceptualization, C.S. and C.D.; methodology, C.S.; software, C.W.; validation, C.D., R.L. and W.T.; formal analysis, C.S. and Y.G; investigation, Y.G. and W.T.; resources, C.D.; data curation, C.S.; writing—original draft preparation, C.S.; writing—review and editing, C.W. and M.J.; visualization, C.S., C.W. and M.Y.; funding acquisition, C.D. All authors have read and agreed to the published version of the manuscript.

Funding: This research was funded by the National Natural Science Foundation of China, the State Key Laboratory of Permafrost Engineering Open Fund Grant and the Strategic Priority Research Program of the Chinese Academy of Sciences, and numbers are as follows: National Natural Science Foundation of China, No. 41202171, The State Key Laboratory of Permafrost Engineering Open Fund Grant, No. SKLFSE201310, the Strategic Priority Research Program of the Chinese Academy of Sciences, No. XDA28100105.

Institutional Review Board Statement: Not applicable.

Informed Consent Statement: Not applicable.

Data Availability Statement: The data presented in this study are openly available, can be downloaded at: The meteorological data, http://data.cma.cn/ (accessed on 28 July 2022); the remote sensing data, https://doi.org/10.24381/cds.68d2bb30 (accessed on 15 August 2022).

Conflicts of Interest: The authors declare no conflict of interest.

References

1. Gregory, J.M.; Stouffer, R.J.; Molina, M.J.; Chidthaisong, A.; Solomon, S.; Raga, G.B.; Friedlingstein, P.; Bindoff, N.L.; Treut, H.L.; Rusticucci, M.; et al. *Climate Change 2021—The Physical Science Basis*; IPCC: Geneva, Switzerland, 2021.
2. IPCC. *Climate Change 2013—The Physical Science Basis: Working Group I Contribution to the Fifth Assessment Report of the Intergovernmental Panel on Climate Change*; Cambridge University Press: Cambridge, UK, 2014.
3. Hoelzle, M.; Chinn, T.; Stumm, D.; Paul, F.; Zemp, M.; Haeberli, W. The application of glacier inventory data for estimating past climate change effects on mountain glaciers: A comparison between the European Alps and the Southern Alps of New Zealand. *Glob. Planet. Chang.* **2007**, *56*, 69–82. [CrossRef]
4. Wei, Z.; Jin, H.; Zhang, J.; Yu, S.; Han, X.; Ji, Y.; He, R.; Chang, X. Prediction of permafrost changes in Northeastern China under a changing climate. *Sci. China Earth Sci.* **2011**, *54*, 924–935. [CrossRef]
5. Zhang, Z.; Wu, Q.; Xun, X.; Li, Y. Spatial distribution and changes of Xing'an permafrost in China over the past three decades. *Quat. Int.* **2019**, *523*, 16–24.
6. Jin, H.; Yu, Q.; Lü, L.; Guo, D.; He, R.; Yu, S.; Sun, G.; Li, Y. Degradation of permafrost in the Xing'anling Mountains, northeastern China. *Permafr. Periglac. Process.* **2007**, *18*, 245–258. [CrossRef]
7. Wang, F.; Li, G.; Ma, W.; Mu, Y.; Zhou, Z.; Mao, Y. Permafrost thawing along the China-Russia Crude Oil Pipeline and countermeasures: A case study in Jiagedaqi, Northeast China. *Cold Reg. Sci. Technol.* **2018**, *155*, 308–313. [CrossRef]
8. Li, X.; Jin, X.; Wang, X.; Jin, H.; Tang, L.; Li, X.; He, R.; Li, Y.; Huang, C.; Zhang, S. Investigation of permafrost engineering geological environment with electrical resistivity tomography: A case study along the China-Russia crude oil pipelines. *Eng. Geol.* **2021**, *291*, 106237. [CrossRef]

9. Dong, X.; Liu, C.; Li, M.; Ma, D.; Chen, Q.; Zang, S. Variations in active layer soil hydrothermal dynamics of typical wetlands in permafrost region in the Great Hing'an Mountains, northeast China. *Ecol. Indic.* **2021**, *129*, 107880. [CrossRef]
10. Li, X.; Jin, H.; Wang, H.; Jin, X.; Bense, V.F.; Marchenko, S.S.; He, R.; Huang, Y.; Luo, D. Effects of fire history on thermal regimes of permafrost in the northern Da Xing'anling Mountains, NE China. *Geoderma* **2022**, *410*, 115670. [CrossRef]
11. He, R.-X.; Jin, H.-J.; Luo, D.-L.; Li, X.-Y.; Zhou, C.-F.; Jia, N.; Jin, X.-Y.; Li, X.-Y.; Che, T.; Yang, X.; et al. Permafrost changes in the Nanwenghe Wetlands Reserve on the southern slope of the Da Xing′anling—Yile′huli mountains, Northeast China. *Adv. Clim. Chang. Res.* **2021**, *12*, 696–709. [CrossRef]
12. Rongali, G.; Keshari, A.K.; Gosain, A.K.; Khosa, R. Split-Window Algorithm for Retrieval of Land Surface Temperature Using Landsat 8 Thermal Infrared Data. *J. Geovisualization Spat. Anal.* **2018**, *2*, 14. [CrossRef]
13. Luo, D.; Jin, H.; Marchenko, S.S.; Romanovsky, V.E. Difference between near-surface air, land surface and ground surface temperatures and their influences on the frozen ground on the Qinghai-Tibet Plateau. *Geoderma* **2018**, *312*, 74–85. [CrossRef]
14. Frauenfeld, O.W.; Zhang, T.; Mccreight, J.L. Northern Hemisphere freezing/thawing index variations over the twentieth century. *Int. J. Clim.* **2006**, *27*, 47–63. [CrossRef]
15. Peng, X.; Zhang, T.; Liu, Y.; Luo, J. Past and Projected Freezing/Thawing Indices in the Northern Hemisphere. *J. Appl. Meteorol. Clim.* **2019**, *58*, 495–510. [CrossRef]
16. Peng, X.; Zhang, T.; Cao, B.; Wang, Q.; Wang, K.; Shao, W.; Guo, H. Changes in Freezing-Thawing Index and Soil Freeze Depth Over the Heihe River Basin, Western China. *Arct. Antarct. Alp. Res.* **2016**, *48*, 161–176. [CrossRef]
17. Nelson Frederick, E. (Un) frozen in Time. *Science* **2003**, *299*, 1673–1675. [CrossRef]
18. Nelson, F.E.; Outcalt, S.I. A Computational Method for Prediction and Regionalization of Permafrost. *Arct. Alp. Res.* **1987**, *19*, 279. [CrossRef]
19. Zhang, Z.; Wu, Q.; Xun, X.; Wang, B.; Wang, X. Climate change and the distribution of frozen soil in 1980–2010 in northern northeast China. *Quat. Int.* **2018**, *467*, 230–241. [CrossRef]
20. Wu, Q.; Liu, Y. Ground temperature monitoring and its recent change in Qinghai–Tibet Plateau. *Cold Reg. Sci. Technol.* **2004**, *38*, 85–92.
21. Klene, A.E.; Nelson, F.E.; Shiklomanov, N.I.; Hinkel, K.M. The N-factor in Natural Landscapes: Variability of Air and Soil-Surface Temperatures, Kuparuk River Basin, Alaska, U.S.A. *Arct. Antarct. Alp. Res.* **2001**, *33*, 140–148. [CrossRef]
22. Yin, G.; Niu, F.; Lin, Z.; Luo, J.; Liu, M. Effects of local factors and climate on permafrost conditions and distribution in Beiluhe basin, Qinghai-Tibet Plateau, China. *Sci. Total Environ.* **2017**, *581–582*, 472–485. [CrossRef]
23. Luo, D.; Liu, L.; Jin, H.; Wang, X.; Chen, F. Characteristics of ground surface temperature at Chalaping in the Source Area of the Yellow River, northeastern Tibetan Plateau. *Agric. For. Meteorol.* **2019**, *281*, 107819. [CrossRef]
24. Aalto, J.; Karjalainen, O.; Hjort, J.; Luoto, M. Statistical Forecasting of Current and Future Circum-Arctic Ground Temperatures and Active Layer Thickness. *Geophys. Res. Lett.* **2018**, *45*, 4889–4898. [CrossRef]
25. Peng, X.; Zhang, T.; Frauenfeld, O.W.; Wang, K.; Cao, B.; Zhong, X.; Su, H.; Mu, C. Response of seasonal soil freeze depth to climate change across China. *Cryosphere* **2017**, *11*, 1059–1073. [CrossRef]
26. Shi, Y.; Niu, F.; Lin, Z.; Luo, J. Freezing/thawing index variations over the circum-Arctic from 1901 to 2015 and the permafrost extent. *Sci. Total Environ.* **2019**, *660*, 1294–1305. [CrossRef] [PubMed]
27. Zhang, T.; Frauenfeld, O.W.; Serreze, M.C.; Etringer, A.; Oelke, C.; McCreight, J.L.; Barry, R.; A Gilichinsky, D.; Yang, D.; Ye, H.; et al. Spatial and temporal variability in active layer thickness over the Russian Arctic drainage basin. *J. Geophys. Res. Atmos.* **2005**, *110*, 1–14. [CrossRef]
28. Wu, T.; Wang, Q.; Zhao, L.; Batkhishig, O.; Watanabe, M. Observed trends in surface freezing/thawing index over the period 1987–2005 in Mongolia. *Cold Reg. Sci. Technol.* **2011**, *69*, 105–111. [CrossRef]
29. Wu, Q.; Zhang, T. Recent permafrost warming on the Qinghai-Tibetan Plateau. *J. Geophys. Res. Atmos.* **2008**, *113*, D13108. [CrossRef]
30. Frauenfeld, O.W.; Zhang, T.; Barry, R.; Gilichinsky, D. Interdecadal changes in seasonal freeze and thaw depths in Russia. *J. Geophys. Res. Earth Surf.* **2004**, *109*, D05101. [CrossRef]
31. Shan, W.; Zhang, C.; Guo, Y.; Qiu, L. Mapping the Thermal State of Permafrost in Northeast China Based on the Surface Frost Number Model. *Remote Sens.* **2022**, *14*, 3185. [CrossRef]
32. Shan, W.; Zhang, C.; Guo, Y.; Qiu, L.; Xu, Z.; Wang, Y. Spatial Distribution and Variation Characteristics of Permafrost Temperature in Northeast China. *Sustainability* **2022**, *14*, 8178. [CrossRef]
33. Xu, S.; Liu, D.; Li, T.; Fu, Q.; Liu, D.; Hou, R.; Meng, F.; Li, M.; Li, Q. Spatiotemporal evolution of the maximum freezing depth of seasonally frozen ground and permafrost continuity in historical and future periods in Heilongjiang Province, China. *Atmospheric Res.* **2022**, *274*, 106195. [CrossRef]
34. Song, C.; Dai, C.; Wang, C.; Yu, M.; Gao, Y.; Tu, W. Characteristic Analysis of the Spatio-Temporal Distribution of Key Variables of the Soil Freeze–Thaw Processes over Heilongjiang Province, China. *Water* **2022**, *14*, 2573. [CrossRef]
35. Wang, C.; Shan, M.; Hu, Z.; Shan, W. Multi-spectral remote sensing based land surface temperature retrieval and isolated permafrost zone segmentation. *Infrared Laser Eng.* **2015**, *44*, 1390–1396.
36. Shi, P.; Sun, S.; Wang, M.; Li, N.; Wang, J.A.; Jin, Y.; Gu, X.; Yin, W. Climate change regionalization in China (1961–2010). *Sci. China Earth Sci.* **2014**, *57*, 2676–2689. [CrossRef]

37. Zuo, H.; Lyu, S.; Hu, Y. Variations trend of yearly mean air temperature and precipitation in China in the last 50 years. *Plateau Meteorology* **2004**, *23*, 238–244.
38. He, W.; Bu, R.; Xiong, Z.; Hu, Y. Characteristics of temperature and precipitation in Northeastern China from 1961 to 2005. *Acta Ecol. Sin.* **2013**, *33*, 519–531. [CrossRef]
39. Holben, B.N. Characteristics of maximum-value composite images from temporal AVHRR data. *Int. J. Remote Sens.* **1986**, *7*, 1417–1434. [CrossRef]
40. Pinzon, J.E.; Tucker, C.J. A non-stationary 1981–2012 AVHRR NDVI3g time series. *Remote Sens.* **2014**, *6*, 6929–6960. [CrossRef]
41. Myneni, R.B.; Hall, F.G.; Sellers, P.J.; Marshak, A.L. The interpretation of spectral vegetation indexes. *IEEE Trans. Geosci. Remote Sens.* **1995**, *33*, 481–486. [CrossRef]
42. Chang, X.L.; Jin, H.; He, R. Advances in permafrost and cold regions environments studies in the Da Xing'anling Mountains, Northeastern China. *J. Glaciol. Geocryol.* **2008**, *30*, 176–182.
43. Jin, H.; Li, S.; Cheng, G.; Shaoling, W.; Li, X. Permafrost and climatic change in China. *Glob. Planet. Chang.* **2000**, *26*, 387–404. [CrossRef]
44. Zhang, Z.-Q.; Wu, Q.-B.; Hou, M.-T.; Tai, B.-W.; An, Y.-K. Permafrost change in Northeast China in the 1950s–2010s. *Adv. Clim. Chang. Res.* **2021**, *12*, 18–28. [CrossRef]
45. Wang, X.; Chen, R.; Liu, G.; Yang, Y.; Song, Y.; Liu, J.; Liu, Z.; Han, C.; Liu, X.; Guo, S.; et al. Spatial distributions and temporal variations of the near-surface soil freeze state across China under climate change. *Glob. Planet. Chang.* **2018**, *172*, 150–158. [CrossRef]
46. Fu, Q.; Zhou, Z.; Li, T.; Liu, D.; Hou, R.; Cui, S.; Yan, P. Spatiotemporal characteristics of droughts and floods in northeastern China and their impacts on agriculture. *Stoch. Environ. Res. Risk Assess.* **2018**, *32*, 2913–2931. [CrossRef]
47. Pei, W.; Fu, Q.; Liu, D.; Li, T.-X.; Cheng, K.; Cui, S. Spatiotemporal analysis of the agricultural drought risk in Heilongjiang Province, China. *Theor. Appl. Clim.* **2018**, *133*, 151–164. [CrossRef]
48. Zhou, Z.; Ding, Y.; Shi, H.; Cai, H.; Fu, Q.; Liu, S.; Li, T. Analysis and prediction of vegetation dynamic changes in China: Past, present and future. *Ecol. Indic.* **2020**, *117*, 106642. [CrossRef]
49. Luo, D.; Jin, H.; Jin, R.; Yang, X.; Lü, L. Spatiotemporal variations of climate warming in northern Northeast China as indicated by freezing and thawing indices. *Quat. Int.* **2014**, *349*, 187–195. [CrossRef]
50. Wang, R.; Zhu, Q.; Ma, H. Changes in freezing and thawing indices over the source region of the Yellow River from 1980 to 2014. *J. For. Res.* **2019**, *30*, 257–268. [CrossRef]
51. Gocic, M.; Trajkovic, S. Analysis of changes in meteorological variables using Mann-Kendall and Sen's slope estimator statistical tests in Serbia. *Glob. Planet. Chang.* **2013**, *100*, 172–182. [CrossRef]
52. Longo-Minnolo, G.; Vanella, D.; Consoli, S.; Pappalardo, S.; Ramírez-Cuesta, J.M. Assessing the use of ERA5-Land reanalysis and spatial interpolation methods for retrieving precipitation estimates at basin scale. *Atmospheric Res.* **2022**, *271*, 106131. [CrossRef]
53. Fedorov, A.; Konstantinov, P.; Vasilyev, N.; Shestakova, A. The influence of boreal forest dynamics on the current state of permafrost in Central Yakutia. *Polar Sci.* **2019**, *22*, 100483. [CrossRef]
54. Xu, S.; Fu, Q.; Li, T.; Meng, F.; Liu, D.; Hou, R.; Li, M.; Li, Q. Spatiotemporal characteristics of the soil freeze-thaw state and its variation under different land use types—A case study in Northeast China. *Agric. For. Meteorol.* **2021**, *312*, 108737. [CrossRef]
55. Smith, M.W.; Riseborough, D.W. Climate and the limits of permafrost: A zonal analysis. *Permafr. Periglac. Process.* **2002**, *13*, 1–15. [CrossRef]
56. Luo, D.; Jin, H.; Lü, L.; Zhou, J. Spatiotemporal changes in extreme ground surface temperatures and the relationship with air temperatures in the Three-River Source Regions during 1980–2013. *Theor. Appl. Clim.* **2016**, *123*, 885–897. [CrossRef]
57. Zhan, M.-J.; Xia, L.; Zhan, L.; Wang, Y. Recognition of Changes in Air and Soil Temperatures at a Station Typical of China's Subtropical Monsoon Region (1961–2018). *Adv. Meteorol.* **2019**, *2019*, 6927045. [CrossRef]
58. Pan, Y.; Xiao, H.; Xin, Z.; Li, J.; Miri, A.; Cao, Q. Characteristics of Energy Distribution in a Desert Ecosystem in Inner Mongolia, Northern China. *Front. Environ. Sci.* **2022**, *10*, 939782. [CrossRef]
59. Zhu, M.; Liu, D.; Tang, W.; Chi, Q.; Zhao, X.; Xu, S.; Ye, S.; Wang, Y.; Cui, Y.; Zhou, S. Exploring the Ecological Climate Effects Based on Five Land Use Types: A Case Study of the Huang-Huai-Hai River Basin in China. *Land* **2022**, *11*, 265. [CrossRef]
60. Gao, Z.; Horton, R.; Liu, H.P. Impact of wave phase difference between soil surface heat flux and soil surface temperature on soil surface energy balance closure. *J. Geophys. Res. Atmos.* **2010**, *115*, D16112. [CrossRef]
61. Zhang, Q.; Li, H.; Zhao, J. Modification of the land surface energy balance relationship by introducing vertical sensible heat advection and soil heat storage over the Loess Plateau. *Sci. China Earth Sci.* **2012**, *55*, 580–589. [CrossRef]
62. Wang, Q.; Zhang, T.; Jin, H.; Cao, B.; Peng, X.; Wang, K.; Li, L.; Guo, H.; Liu, J.; Cao, L. Observational study on the active layer freeze–thaw cycle in the upper reaches of the Heihe River of the north-eastern Qinghai-Tibet Plateau. *Quat. Int.* **2016**, *440*, 13–22. [CrossRef]
63. Guo, W.; Liu, H.; Anenkhonov, O.A.; Shangguan, H.; Sandanov, D.V.; Korolyuk, A.Y.; Hu, G.; Wu, X. Vegetation can strongly regulate permafrost degradation at its southern edge through changing surface freeze-thaw processes. *Agric. For. Meteorol.* **2018**, *252*, 10–17. [CrossRef]
64. Way, R.G.; Lapalme, C.M. Does tall vegetation warm or cool the ground surface? Constraining the ground thermal impacts of upright vegetation in northern environments. *Environ. Res. Lett.* **2021**, *16*, 054077. [CrossRef]

65. Shen, X.; Liu, B.; Li, G.; Yu, P.; Zhou, D. Impacts of grassland types and vegetation cover changes on surface air temperature in the regions of temperate grassland of China. *Theor. Appl. Climatol.* **2016**, *126*, 141–150. [CrossRef]
66. Shen, X.; Liu, Y.; Wu, L.; Ma, R.; Wang, Y.; Zhang, J.; Wang, L.; Liu, B.; Lu, X.; Jiang, M. Grassland greening impacts on global land surface temperature. *Sci. Total. Environ.* **2022**, *838*, 155851. [CrossRef] [PubMed]
67. Wi, L.; Zhang, J.; Dong, W. Vegetation effects on mean daily maximum and minimum surface air temperatures over China. *Chin. Sci. Bull.* **2011**, *56*, 900–905. [CrossRef]
68. Sharkhuu, N.; Sharkhuu, A. Effects of Climate Warming and Vegetation Cover on Permafrost of Mongolia. In *Eurasian Steppes. Ecological Problems and Livelihoods in a Changing World*; Werger, M.J.A., van Staalduinen, M.A., Eds.; Springer: Dordrecht, The Netherlands, 2012; pp. 445–472.
69. Duveiller, G.; Hooker, J.; Cescatti, A. The mark of vegetation change on Earth's surface energy balance. *Nat. Commun.* **2018**, *9*, 679. [CrossRef]
70. Throop, J.; Lewkowicz, A.G.; Smith, S.L. Climate and ground temperature relations at sites across the continuous and discontinuous permafrost zones, northern Canada. *Can. J. Earth Sci.* **2012**, *49*, 865–876. [CrossRef]
71. Zhang, T. Influence of the seasonal snow cover on the ground thermal regime: An overview. *Rev. Geophys.* **2005**, *43*, RG4002. [CrossRef]
72. Vasil'ev, I.S.; Vasil'ev, A.I.; Torgovkin, Y.I. Air freezing and thawing indices in Yakutia and their mapping. *Russ. Meteorol. Hydrol.* **2012**, *37*, 170–176. [CrossRef]
73. Wu, T.; Zhu, X.; Wang, P.; Adiya, S.; Avirmed, D.; Dorjgotov, B.; Li, R.; Wu, X.; Lou, P. Climate warming in the Qinghai-Tibet Plateau and Mongolia as indicated by air freezing and thawing indices. *Ecol. Indic.* **2022**, *138*, 108836. [CrossRef]
74. Qi, F.; Zhang, M.; Lu, S.; Bai, Y.; Yang, W. *Quaternary Geology of Sanjiang Plain*; Geological Press: Beijing, China, 2015.
75. Zhou, X.; Zhao, C.; Li, N.; Liu, M.; Cui, Y.; Ao, X. Influence of snow and temperature on the depth of frozen soil in winter half year in Northeast China. *J. Glaciol. Geocryol.* **2021**, *43*, 1027–1039.
76. Liu, S.; Zang, S.; Zhang, L.; Na, X. Estimation of land surface temperature from MODIS in Northeast China. *Geogr. Res.* **2017**, *36*, 2251–2260.
77. Zhao, J.-Y.; Chen, J.; Wu, Q.-B.; Hou, X. Snow cover influences the thermal regime of active layer in Urumqi River Source, Tianshan Mountains, China. *J. Mt. Sci.* **2018**, *15*, 2622–2636. [CrossRef]
78. Chang, X.; Jin, H.; Yu, S.; Sun, H.; He, R.; Luo, D.; Sun, G.; Lu, L. Influence of vegetation on frozen ground temperatures the forested area in the Da Xing'anling Mountains, Northeastern China. *Shengtai Xuebao/Acta Ecol. Sin.* **2011**, *31*, 5138–5147.
79. Wang, Y.; Jin, H.; Li, G. Investigation of the freeze–thaw states of foundation soils in permafrost areas along the China–Russia Crude Oil Pipeline (CRCOP) route using ground-penetrating radar (GPR). *Cold Reg. Sci. Technol.* **2016**, *126*, 10–21. [CrossRef]
80. Li, X.; Jin, H.; He, R.; Huang, Y.; Wang, H.; Luo, D.; Jin, X.; Lü, L.; Wang, L.; Li, W.; et al. Effects of forest fires on the permafrost environment in the northern Da Xing'anling (Hinggan) mountains, Northeast China. *Permafr. Periglac. Process.* **2019**, *30*, 163–177. [CrossRef]
81. Boike, J.; Grau, T.; Heim, B.; Günther, F.; Langer, M.; Muster, S.; Gouttevin, I.; Lange, S. Satellite-derived changes in the permafrost landscape of central Yakutia, 2000–2011: Wetting, drying, and fires. *Glob. Planet. Chang.* **2016**, *139*, 116–127. [CrossRef]